machines

MDPI

Article

Topology Optimization and Stiffener Reconstruction of a Ram-Boring Spindle Assembly in a Floor-Type Milling and Boring Machine for Deformation Control Under Large Extension

Donghui Xu [1,*], Yanqi Guan [1], Chongmin Jiang [2] and Rui Fan [1]

[1] School of Mechanical and Electrical Engineering, Qiqihar University, Qiqihar 161000, China; guanyq12345@163.com (Y.G.); fanrui_2325@163.com (R.F.)
[2] Genertec Qiqihar No. 2 Machine Tool Co., Ltd., No. 371 Yong'an Street, Longsha District, Qiqihar 161000, China; jiangchongmin@q2jc.gt.cn
* Correspondence: xu.donghui@qqhru.edu.cn

Abstract

To reduce ram deflection and positional deviation at the boring spindle front end of a floor-type milling and boring machine under large extension, a ram-boring spindle assembly was investigated. A finite element model was established based on the actual structure, guideway support, and spindle assembly. Gravity-induced deformation and vertical displacement at the boring spindle front end under different extension conditions were analyzed to identify weak regions. The Solid Isotropic Material with Penalization method was then used to optimize the adjustable internal region of the ram with the objective of reducing structural compliance. The topology–density distribution and the deformation characteristics under different extension conditions were then used to guide an engineering reconstruction of the internal stiffeners, considering casting, assembly, internal space constraints, and engineering experience. Static analysis, displacement testing, and modal analysis were performed to verify the optimized structure. Results show that the maximum total deformation under simultaneous maximum extension decreased from 0.10268 mm to 0.097325 mm, while the mass decreased from 2424 kg to 2363 kg. The measured vertical displacement decreased from 0.114 mm to 0.108 mm. The first six natural frequencies increased by 1.48–5.91%. The proposed reconstruction improves deformation control and dynamic performance while reducing mass.

Keywords: floor-type milling and boring machine; ram structure; topology optimization; stiffener reconstruction; end deformation control

Check for updates

Academic Editor: Panagiotis Kyratsis

Received: 14 July 2026
Revised: 3 August 2026
Accepted: 4 August 2026
Published: 6 August 2026

Copyright: © 2026 by the authors. Licensee MDPI, Basel, Switzerland. This article is an open access article distributed under the terms and conditions of the Creative Commons Attribution (CC BY) license.

1. Introduction

Floor-type milling and boring machines are widely used for the precision machining of large and complex components in energy equipment, aerospace, shipbuilding and heavy machinery industries because of their long machining strokes, high load-bearing capacity, and strong process adaptability. The ram is a key load-bearing and feeding component connecting the spindle system and the machine body, and its structural stiffness and deformation behavior directly affect the position and attitude accuracy of the tool center point. Owing to its box-type thin-walled structure with a large slenderness ratio, the support condition and cantilever characteristics of the ram vary continuously as the extension length increases. Under the combined effects of self-weight, spindle and accessory mass, and cutting loads, the ram is prone to vertical deflection, lateral displacement, and

front-end angular deformation. These deformations may further cause positional deviation at the boring spindle front end and be transmitted to the tool center point through the tool mounting relationship, thereby affecting bore positioning accuracy, coaxiality, and machined surface quality. Therefore, reducing ram deflection and positional deviation at the boring spindle front end while controlling structural mass is important for improving the full-stroke accuracy retention of floor-type milling and boring machines.

Research on deformation and accuracy loss caused by ram extension has mainly focused on deformation prediction and compensation. Early studies on floor-type milling and boring machines mainly addressed ram deflection through mechanical compensation. Wu Fenghe et al. investigated the deflection behavior of a large-stroke ram in a superheavy CNC floor-type milling and boring machine by combining theoretical analysis, finite element calculation, and experimental testing, and established the relationship between compensation force and ram stroke [1]. On this basis, Wu et al. [2] derived the compensation force and moment of a ram assembly based on force and moment equilibrium, and compensated the deformation of the ram and headstock using tie rods, hydrostatic guideway pressure adjustment, and steel wire ropes. To reduce the additional axial deformation introduced by conventional tie-rod compensation, Wu and Zhao [3] further proposed a combined tie-rod and push-rod compensation structure. In addition to mechanical compensation, improving the prediction and correction accuracy of machine tool deformation has also received attention. Han et al. [4] combined self-weight test data with a finite difference model to correct finite element calculation results for large cast-iron structures, thereby improving the prediction accuracy of gravity-induced deformation. More recently, geometric error measurement, modeling, and compensation for CNC machine tools have been systematically reviewed, showing that volumetric error modeling and compensation remain important approaches for improving machining accuracy [5,6]. Thermal error compensation has also developed toward position-dependent and data-driven strategies, especially for multi-axis machine tools with varying thermal boundary conditions [7]. These studies indicate that compensation strategies based on position, load, and temperature states can effectively improve machining accuracy. However, such methods strongly depend on compensation models, sensor accuracy, and actuator stability, and the compensation parameters often need to be re-identified when the ram extension position, accessory mass, or machining state changes. More importantly, compensation methods mainly correct the consequences of structural deformation rather than fundamentally improving the material utilization and bending stiffness of the ram itself.

Compared with compensation methods, structural optimization can improve the load-bearing efficiency of key machine tool components by directly adjusting material distribution and load transfer paths. Traditional structural optimization of machine tools usually takes wall thickness, stiffener dimensions and local geometric parameters as design variables. Bai et al. [8] proposed a multiobjective optimization method for the bed structure of a CNC gantry machine tool based on neural networks and intelligent optimization algorithms, showing that the coordinated optimization of mass, static stiffness, and dynamic characteristics is still an important route for improving machine tool performance. However, parametric optimization is generally based on existing structural configurations and is therefore limited by the initial layout and design experience. To overcome the limitations of predefined structural forms, topology optimization has been increasingly applied to the structural design of machine tool components. Lin and Chang [9] improved the stiffness of a machine tool structure through topology optimization based on machining characteristics, and showed that topology-derived structures can enhance stiffness while maintaining reasonable structural mass. Behera et al. [10] further used topology optimization to improve the structural and dynamic performance of a high-precision five-axis

machine tool, indicating that topology-based design can be used to improve the stiffness and dynamic characteristics of complex machine tool structures. With the increasing demand for high-speed and high-precision machining, structural optimization has gradually shifted from static stiffness improvement to the coordinated enhancement of static and dynamic performance. Liu et al. [11] proposed a ground-structure-method-based stiffener layout topology optimization method for a horizontal machining center headstock cover plate, in which the stiffener layout was optimized by maximizing the natural frequency, and the first six natural frequencies were effectively improved. In addition, recent studies on CNC gantry machine tools and machine tool moving structures have further confirmed that finite element analysis, topology optimization and intelligent optimization algorithms can be combined to improve lightweight performance, stiffness and modal characteristics [8,12]. These studies indicate that topology optimization provides an effective way to generate more reasonable material layouts than conventional size optimization. However, topology optimization results are often obtained as irregular material density distributions, and they still need to be transformed into manufacturable stiffener structures that satisfy casting, assembly and internal space constraints. Moreover, for machine tool components with obvious dynamic requirements, low-order modal performance should also be considered during structural reconstruction.

Although recent studies have established a relatively complete route from weak-region identification and topological configuration generation to manufacturable structural reconstruction and performance validation, most investigated objects are machine beds, columns, headstocks, cross rails and worktables with fixed or relatively stable support conditions [8–12]. For example, Liu et al. [11] optimized the stiffener layout of a horizontal machining center headstock cover plate by maximizing the natural frequency, while Lin and Chang [9] and Behera et al. [10] improved the stiffness and dynamic performance of machine tool structures through topology-based structural optimization. However, these components differ from the ram of a floor-type milling and boring machine, whose overhanging length, gravity-induced bending moment and guideway support state vary continuously during extension. Wang et al. [13] proposed a static precision design method for heavy-duty vertical machining centers based on gravity deformation error modelling, but the investigated structure had a relatively stable support relationship. Bilgili et al. [14] and Liu and Altintas [15] further showed that the dynamic behavior of machine tools can be strongly position dependent, indicating that the structural response of machine tools should be evaluated under changing configurations rather than under a single fixed posture. Zhuang et al. [16] also demonstrated that machine tool support stiffness is affected by structural weight and support reaction, suggesting that the equivalent boundary condition of a guideway-supported component should be treated carefully when the load distribution changes during motion.

For topology optimization, the optimized material density field usually contains discontinuous or irregular features and cannot be directly used as a manufacturable engineering structure. Jin et al. [17] proposed a parametric reconstruction method for topology optimization results of curved stiffened structures, showing that topology-derived density fields need to be converted into explicit geometric features before detailed design and manufacturing. Busch et al. [18] also pointed out that deriving parametric CAD geometries from topology optimization results is time consuming and that topology-optimized structures should be transformed into production-oriented lightweight designs. In addition, Guo [19] noted that large components and large machine equipment are prone to deformation and require high-precision machining and measurement strategies, while Wang et al. [20] emphasized that geometric accuracy design of CNC machine tools involves the coupled consideration of modeling, analysis, optimization and accuracy verification. Taguchi methods

and artificial-neural-network-assisted approaches have also been applied to engineering optimization and performance prediction [21,22]. Related studies have also investigated the integration of geometric and servo-dynamic errors, correlation modeling of intra-axis errors, temperature-distribution modeling during milling, and compensation of trajectory errors in high-speed end-mill boring, further demonstrating the importance of multi-source error modeling and compensation in improving CNC machining accuracy [23–27]. Therefore, for the ram of a floor-type milling and boring machine, evaluating only the maximum deformation or a single compliance value under the fully extended condition is insufficient to characterize its deformation behavior over the operating stroke. It is also necessary to identify the principal regions affecting front-end positional deviation under different extension conditions and to use the topology–density distribution as a guide for subsequent stiffener adjustment. Because the irregular topology result cannot be directly adopted as a cast ram structure, the final stiffener layout must be determined by jointly considering the deformation characteristics, topology result, casting feasibility, assembly requirements, internal installation space and engineering experience. The reconstructed structure should then be verified through static analysis, modal analysis and experimental testing.

Based on the above analysis, this study investigates the ram-boring spindle assembly of a floor-type milling and boring machine, with particular emphasis on gravity-induced deformation, positional deviation at the boring-spindle front end and structural lightweighting under large-extension conditions. First, a finite element model is established based on the actual ram structure, guideway support configuration and spindle-system assembly relationship. Typical operating conditions, including maximum ram extension, maximum boring-spindle extension and simultaneous maximum extension of both components, are analyzed to reveal the stroke-dependent deformation characteristics and identify the principal regions governing front-end positional deviation. Subsequently, the design and non-design domains of the ram are defined, and SIMP topology optimization is performed to obtain the material-density distribution under the representative unfavorable condition. The topology result is then combined with the deformation-analysis results and engineering experience to guide the reconstruction of the internal stiffeners, while the external dimensions, guideway mating surfaces, spindle-mounting regions, casting feasibility, assembly requirements and internal installation space are retained as practical constraints. Finally, the original and reconstructed structures are compared in terms of mass, gravity-induced deformation, boring-spindle front-end displacement and low-order natural frequencies. The reconstructed ram is manufactured, and displacement testing is conducted to verify the effectiveness of the proposed design. Through the integration of stroke-dependent deformation analysis, topology-guided stiffener reconstruction and experimental validation, this study provides a practical engineering approach for improving gravity-induced deformation control and structural lightweighting of large overhanging machine-tool components.

2. Deformation Analysis and Weak Region Identification of the Ram

2.1. Finite Element Model and Extension Conditions of the Ram

The ram-boring spindle assembly of a floor-type milling and boring machine was selected as the research object. It mainly consists of the ram, boring spindle, milling spindle and headstock, as shown in Figure 1. The ram is installed inside the headstock and extends in the axial direction, while the boring spindle and milling spindle are arranged at the front end of the ram, together forming the machining end structure. The ram adopts a closed box-type thin-walled structure. Longitudinal stiffeners are arranged along its length and connected by several transverse stiffeners. Local ring-shaped and reinforced structures are provided near the spindle mounting and guideway support regions to ensure

continuous load transfer inside the ram, as shown in Figure 2. During machining, both the ram and the boring spindle can extend axially. As the overhanging length increases, the system centroid gradually moves away from the headstock, and the ram undergoes obvious bending deformation under its own weight and the mass of the boring spindle and spindle accessories, further causing positional deviations at the ram front end and the boring spindle front end. Since the boring spindle front end is close to the tool mounting position, its displacement can reflect the end positional deviation of the ram-boring spindle assembly under gravity. Therefore, the vertical displacement at the boring spindle front end was used as an important indicator for evaluating the accuracy retention capability of the structure. The stiffener layout and material distribution inside the ram directly determine its bending stiffness and end deformation control capability. Accordingly, the ram-boring spindle assembly was taken as the analysis object. A finite element model was established while retaining the ram shell, main internal stiffeners, guideway support surfaces, spindle mounting regions and other key load-bearing structures, providing the basis for subsequent deformation analysis and topology optimization under different extension conditions.

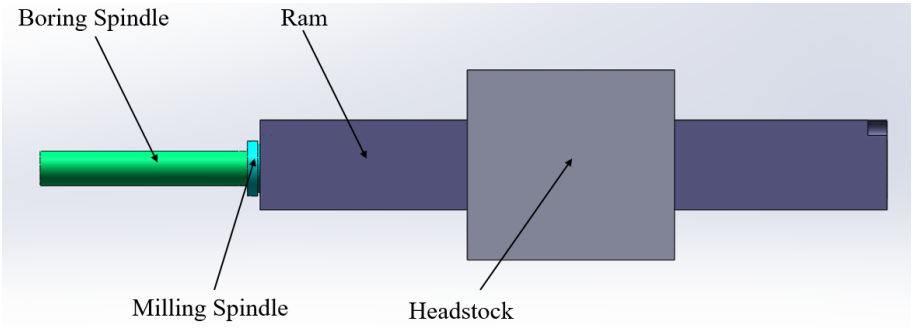


Figure 1. Schematic diagram of the ram assembly of the floor-type milling and boring machine.

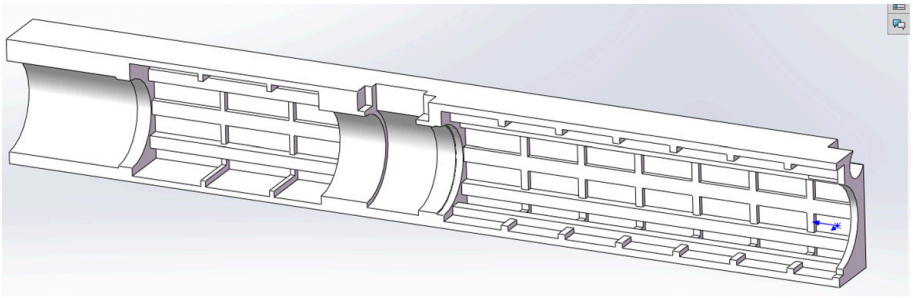


Figure 2. Internal stiffener structure of the original ram.

To improve computational efficiency while retaining the main load-bearing characteristics of the structure, small holes, chamfers and other non-critical geometric details were appropriately simplified without changing the overall load transfer path and sectional stiffness of the ram. A three-dimensional solid finite element model of the ram-boring spindle assembly was then established. According to the actual material properties, the ram was made of QT600-3, with a density of 7250 kg/m^3, an elastic modulus of 172 GPa and a Poisson's ratio of 0.28. The spindle and boring spindle were made of 42CrMo and 38CrMoAlE, respectively, both with a density of 7850 kg/m^3, an elastic modulus of 210 GPa and a Poisson's ratio of 0.29. The finite element analyses were performed using ANSYS Workbench 2024 R1. The mesh method and element type were determined using the Program Controlled option, while a global element size of 20 mm was manually specified. The original model contained 795,674 nodes and 416,386 elements. The ram walls, principal internal stiffeners, guideway-supported regions, and spindle-mounting

regions were retained to represent the global load-transfer path and sectional stiffness. Because the present study focuses on the overall flexural deformation and low-order modal characteristics rather than localized stress concentrations, small holes, chamfers, and other non-critical geometric details were omitted. The same meshing strategy was adopted for all extension conditions. The ram–headstock guideway interface was modeled using bonded contact to represent the overall supporting action of the guideway, while the bottom of the headstock was fully constrained to represent its connection with the machine body. The same boundary-condition scheme was applied to the original and reconstructed models to enable a consistent comparison of their gravity-induced deformation responses. Gravity was applied in the vertical direction so that the self-weight of the ram, spindle and boring spindle was included in the calculation. To compare the deformation behavior under different overhanging conditions, the same material parameters, mesh settings and boundary conditions were adopted for all cases, while only the extension lengths of the ram and boring spindle were changed. The finite element model, boundary conditions and mesh generation are shown in Figure 3.

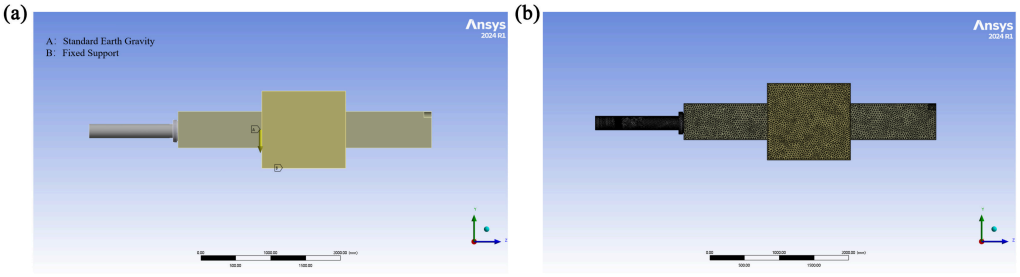


Figure 3. Finite element model of the original structure: (**a**) model and boundary conditions; (**b**) mesh generation.

2.2. Gravity-Induced Deformation and End Displacement Analysis of the Ram

The gravity-induced deformation was first analyzed when the ram and boring spindle both reached their maximum extensions. Under this condition, the overhanging length of the assembly is the largest, and the bending moment caused by the self-weight of the ram, spindle and boring spindle is relatively high. Therefore, this condition can be regarded as a representative unfavorable case for evaluating the accuracy retention capability of the original structure. As shown in Figure 4, the structural deformation gradually increases from the headstock support end to the boring spindle front end. The maximum total deformation occurs at the boring spindle front end, with a value of 0.10268 mm, whereas the deformation near the headstock and guideway support regions is relatively small. The overall displacement distribution exhibits a typical cantilever bending characteristic, indicating that the ram deflection after extension and the downward deformation of the boring spindle are superimposed at the free end and are finally reflected as the positional deviation at the boring spindle front end. Since the boring spindle front end is located at the farthest overhanging end of the assembly and is close to the tool mounting position, its vertical displacement can reflect the end positional deviation of the ram-boring spindle assembly under gravity. Therefore, the simultaneous maximum extension condition of the ram and boring spindle was selected as the key condition for subsequent topology optimization and structural performance comparison.

The vertical displacement of the node at the boring spindle front end under different extension conditions was further extracted from the original structure, as shown in Figure 5. The two curves correspond to two conditions: the boring spindle gradually extends while the ram remains at its maximum extension, and the ram gradually extends while the boring spindle remains at its maximum extension. When the ram was kept at its maximum

extension and the boring spindle was gradually extended from 0 mm to 1200 mm, the vertical displacement at the boring spindle front end increased from 0.019947 mm to 0.10268 mm. With increasing boring spindle extension, the load acting distance at the free end increased continuously, and the downward deformation of the boring spindle front end became more pronounced. The displacement increment was more obvious in the large-extension range, indicating that boring spindle extension significantly amplifies the gravity-induced deformation at the front end of the assembly. When the boring spindle was kept at its maximum extension and the ram was gradually extended from 0 mm to 1200 mm, the vertical displacement at the boring spindle front end increased from 0.038042 mm to 0.10268 mm. In the small-extension range, the displacement increased relatively slowly. As the ram extension continued to increase, the overall overhanging length and bending moment of the structure increased, leading to a marked increase in the vertical displacement at the boring spindle front end. These two groups of results indicate that the end deformation of the ram-boring spindle assembly is closely related to the extension length. In particular, under large overhanging conditions, the vertical displacement at the boring spindle front end becomes more sensitive to the structural extension length. Therefore, the bending stiffness of the ram body and its internal load transfer path are key factors affecting the full-stroke accuracy retention capability of the assembly. The subsequent optimization should focus on improving the material distribution and stiffener connection form of the ram under large-extension conditions.

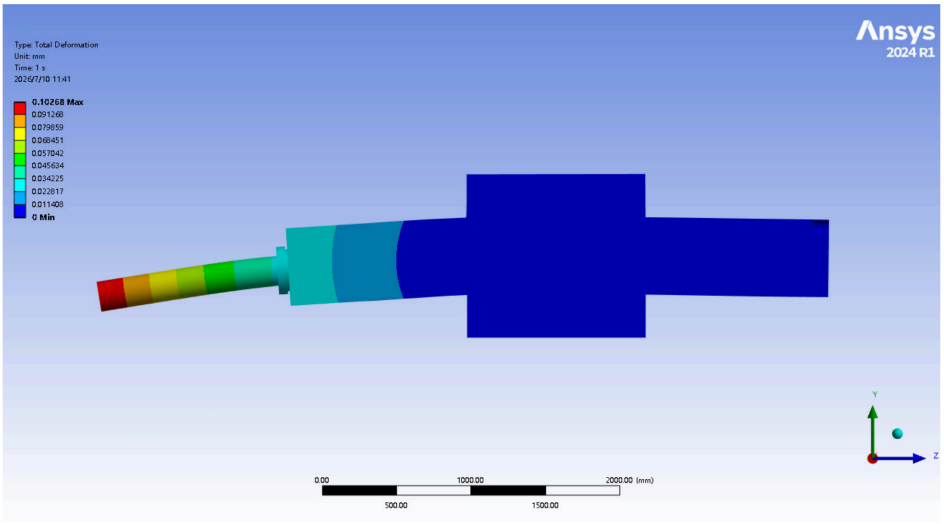


Figure 4. Gravity-induced deformation contour of the original model when the ram and boring spindle are both fully extended.

The two displacement curves both reach 0.10268 mm when the ram and boring spindle are simultaneously extended to their maximum positions, confirming this configuration as a representative unfavorable condition for subsequent structural optimization. The selection of the ram as the optimization object was determined by its structural function and available design space. As the principal load-bearing and feeding component connecting the headstock and the spindle system, the ram supports its own weight together with the masses of the milling spindle, boring spindle and associated components. During extension, the guideway-supported length and overhanging length of the ram change continuously, directly affecting the global bending load-transfer path and the transmission of gravity-induced deformation to the boring-spindle front end.

The boring spindle is a precision rotating functional component whose external geometry, mounting relationship and transmission interfaces are subject to strict functional

constraints, leaving limited space for structural modification. In contrast, the ram is a box-type thin-walled casting with adjustable internal cavities and stiffeners. Its internal material distribution and stiffener connections can be modified while retaining the external profile, guideway mating surfaces and spindle-mounting interfaces. Therefore, the adjustable internal region of the ram was selected as the main design domain for topology optimization, with the objectives of reducing the vertical displacement at the boring-spindle front end and the gravity-induced deformation of the assembly under large-extension conditions. Structural mass and low-order natural frequencies were also considered to avoid increasing the structural mass or degrading the dynamic performance while improving deformation control.

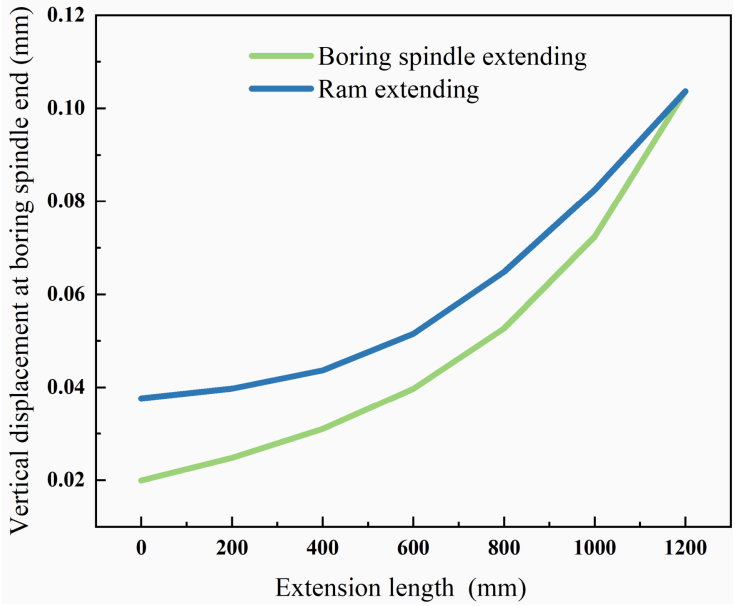


Figure 5. Variation in vertical displacement at the boring spindle front end under different extension conditions.

3. Topology Optimization and Structural Design of the Ram

3.1. Initial Structural Design Based on Topology Optimization

According to the deformation analysis of the original structure in Section 2, the flexural deformation of the ram under large-extension conditions is mainly affected by the internal material distribution and the stiffener load transfer path. To improve the bending stiffness without changing the external dimensions, guideway matching relationship and spindle mounting requirements of the ram, topology optimization was adopted to redistribute the material in the adjustable internal region of the ram. In the topology optimization model, the ram outer wall, guideway contact surfaces, spindle and boring spindle mounting regions, end connection regions and other regions affecting assembly datums and motion accuracy were defined as non-design domains, so as to ensure that the key functional surfaces and connection relationships remained unchanged during optimization. The original internal stiffeners and cavity regions where material redistribution was allowed were defined as design domains, enabling the optimization calculation to retain or remove material automatically according to load transfer requirements. The design and non-design domains are shown in Figure 6. Through this treatment, the topology optimization can reflect the main load transfer path of the ram under gravity while ensuring the feasibility of subsequent engineering reconstruction and manufacturing.

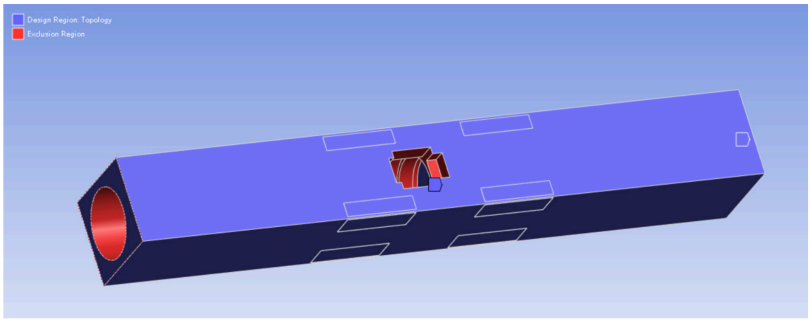


Figure 6. Design and non-design domains for topology optimization of the ram.

The variable density method was used for topology optimization. The relative density of each finite element in the design domain was taken as the design variable, and the removal or retention of material was represented by the continuous variation of material density between 0 and 1. The relative density of the *i*-th element, ρ_i, is defined as:

$$0 < \rho_{\min} \leq \rho_i \leq 1 \tag{1}$$

where $\rho_i = 1$ indicates that the element is retained as solid material, whereas ρ_i close to 0 indicates that the material in the element is removed. To reduce the influence of intermediate-density elements on the optimization result, the SIMP interpolation model was adopted to describe the relationship between the elastic modulus and relative density of each element:

$$E_i(\rho_i) = E_{\min} + \rho_i^p (E_0 - E_{\min}) \tag{2}$$

where E_i is the equivalent elastic modulus of the *i*-th element, E_0 is the elastic modulus of the solid material, E_{min} is a small elastic modulus introduced to avoid singularity of the stiffness matrix, and p is the penalization factor. The penalization factor reduces the stiffness contribution of intermediate-density elements and promotes a 0–1 material distribution, thereby facilitating subsequent engineering stiffener reconstruction.

A retained mass fraction of 30% was specified in the topology optimization, corresponding to a material volume fraction of 30% for the single-material design domain. The numerical controls for the density-based topology optimization, including the SIMP penalization, minimum-stiffness, filtering, convergence, and maximum-iteration settings, were left at the Program Controlled settings in ANSYS Workbench 2024 R1.

In this study, structural compliance under the density-dependent gravity field was selected as the optimization objective, so that material was preferentially retained in regions that contributed significantly to the deformation control of the ram. The structural compliance and equilibrium equation are expressed as:

$$\begin{cases} C(\rho) = \mathbf{F}^T(\rho)\mathbf{u}(\rho) \\ \mathbf{K}(\rho)\mathbf{u}(\rho) = \mathbf{F}(\rho) \end{cases} \tag{3}$$

where $C(\rho)$ is the structural compliance, $\mathbf{K}(\rho)$ is the density-dependent global stiffness matrix, and $\mathbf{u}(\rho)$ is the displacement vector, *and* $\mathbf{F}(\rho)$ is the density-dependent load vector. The load vector can be expressed as:

$$\mathbf{F}(\boldsymbol{\rho}) = \mathbf{F}_{\text{fix}} + \sum_{i=1}^{N} \rho_i \mathbf{f}_{g,i}^0 \tag{4}$$

where $\mathbf{F}_{\text{fix}}$ denotes the gravitational loads of the non-design domains and spindle-system components, and $f^0_{g,i}$ is the gravitational load vector of the i-th design element at full material density.

Therefore, the topology optimization model of the ram is formulated as:

$$\begin{cases} \min_{\rho} \quad C(\rho) = \mathbf{F}^T\mathbf{u} \\ \text{s.t.} \quad \mathbf{K}(\rho)\mathbf{u}(\rho) = \mathbf{F}(\rho) \\ \frac{V(\rho)}{V_0} \leq f \\ 0 < \rho_{\min} \leq \rho_i \leq 1 \end{cases} \tag{5}$$

The optimization model determines the material distribution that minimizes structural compliance under the updated self-weight while satisfying the prescribed material volume constraint.

The topology optimization iteration process is shown in Figure 7. As shown in Figure 7a, the objective function decreased rapidly at the early stage of iteration, dropping from the initial normalized value of 100 to below 10 within the first four iterations. This indicates that inefficient material in the design domain was quickly removed, and the material distribution of the structure changed significantly. Subsequently, the objective function entered a fluctuating decreasing stage, further decreased after the 25th iteration, and gradually converged around the 35th iteration. As shown in Figure 7b, the mass constraint decreased rapidly from the initial value to approximately 30% within the first three iterations and then remained near the prescribed constraint during the subsequent iterations, indicating that the optimization process satisfied the mass reduction requirement. The optimized material density distribution is shown in Figure 8. It can be observed that material is mainly retained in the front section of the ram, near the guideway support region and along the main internal load transfer paths, providing a basis for subsequent stiffener reconstruction.

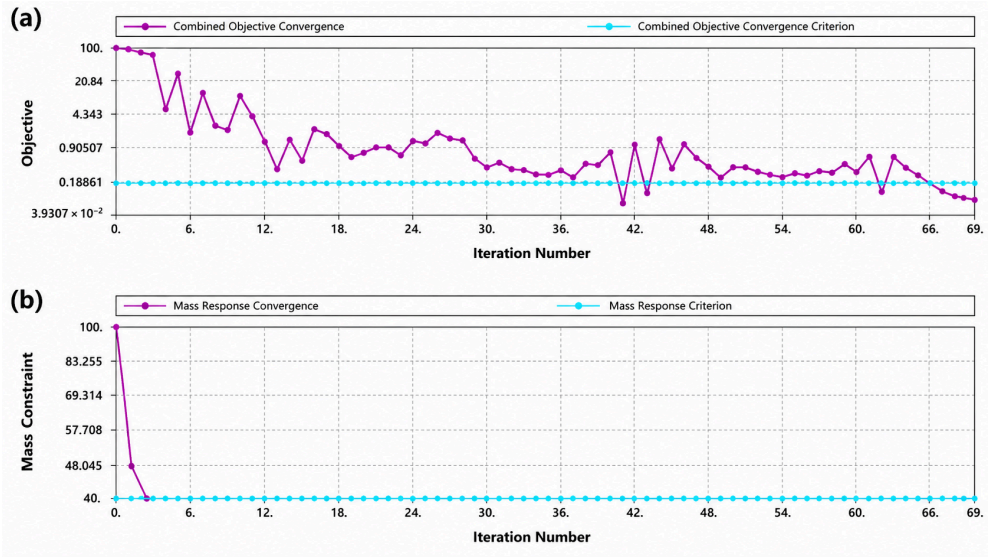


Figure 7. Convergence curves of topology optimization: (**a**) objective function; (**b**) mass constraint.

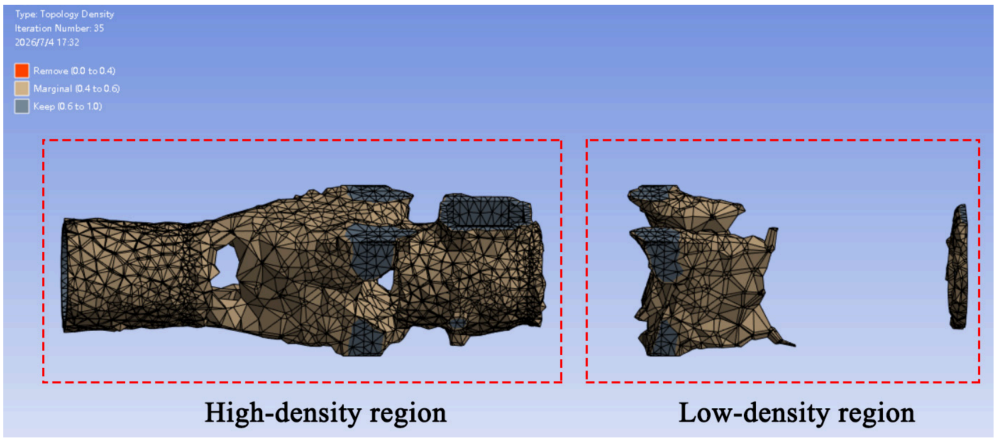


Figure 8. Material density distribution obtained by topology optimization.

3.2. Topology-Guided Engineering Reconstruction of the Ram Stiffeners

The material-density distribution obtained from topology optimization is shown in Figure 8. Relatively continuous high-density regions are concentrated in the front section of the ram and near the guideway-supported region, whereas relatively low-density regions appear in part of the rear section. Together with the stroke-dependent deformation characteristics identified in Section 2, this density distribution indicates that the front overhanging section and the region near the guideway support are important load-transfer regions under gravity. Based on the deformation analysis and topology result, three longitudinal stiffeners and one circular stiffener were added in the front section, while the rear stiffeners were locally thinned and one circular stiffener was removed. The final positions, dimensions and geometric forms of the stiffeners were determined by jointly considering the material-density distribution, engineering experience, casting feasibility, assembly requirements and internal installation space, thereby converting the topology result into a regular and manufacturable stiffener layout.

From the mechanism of topology optimization, the retained material regions are mainly determined by the contribution of each element to the structural compliance. Based on the SIMP interpolation model, the structural compliance can be expressed as the sum of the compliance contributions of all design elements:

$$C = \sum_{i=1}^{N} \rho_i^p \mathbf{u}_i^T \mathbf{k}_0 \mathbf{u}_i \tag{6}$$

where N is the total number of elements in the design domain, ρ_i is the relative density of the i-th element, p is the penalization factor, $\mathbf{u_i}$ is the displacement vector of the i-th element, which varies with the density-dependent stiffness and gravitational load during optimization, and $\mathbf{k_0}$ is the element stiffness matrix corresponding to the solid material. Considering the equilibrium equation constraint, the sensitivity of structural compliance with respect to element density can be expressed as:

$$\frac{\partial C}{\partial \rho_i} = -\mathbf{u}^{\mathrm{T}} \frac{\partial \mathbf{K}}{\partial \rho_i} \mathbf{u} + 2\mathbf{u}^{\mathrm{T}} \frac{\partial \mathbf{F}}{\partial \rho_i} \tag{7}$$

Equation (7) shows that the compliance sensitivity is governed by both the density-dependent stiffness variation and the corresponding change in gravitational load. Therefore, whether material in an element is retained or removed depends on the combined effects of its contribution to structural stiffness and its contribution to self-weight, rather than on the strain-energy term alone. As shown in Figure 8, relatively high-density regions are concentrated in the front section of the ram and near the guideway-supported region, indicating

that density variations in these regions have a relatively significant influence on the structural compliance under the prescribed gravity condition. By contrast, the lower-density regions in the rear section make a smaller contribution to reducing the overall compliance and can therefore be appropriately thinned or locally removed. Accordingly, the subsequent stiffener reconstruction focuses on improving the continuity of the load-transfer path in the front overhanging section while reducing material in the lower-contribution rear regions, thereby balancing gravity-induced deformation control and structural mass reduction.

Based on the above topology optimization results and compliance sensitivity analysis, the internal stiffener structure of the ram was reconstructed, as shown in Figure 9. Compared with the original model, three longitudinal stiffeners were added to the upper and lower positions at the front end of the ram to enhance the bending resistance of the front overhanging section. Meanwhile, an additional circular stiffener was introduced to make the stiffener connection in the front section more continuous, thereby improving the load transfer path from the boring spindle front end to the headstock support region. To control the increase in structural mass, the thickness of the remaining stiffeners was appropriately reduced. For the rear section of the ram, where the material density and compliance sensitivity were relatively low, the stiffener thickness was reduced, and one circular stiffener was removed to decrease the proportion of inefficient material and achieve lightweight optimization. Based on these reconstruction principles, the three-dimensional stiffener structure of the reconstructed ram was established, as shown in Figure 10. It can be seen that, while the external profile, guideway mating surfaces and spindle mounting regions of the ram were retained, the internal stiffener form, local stiffener number and thickness distribution were reconfigured, forming a regular, continuous and manufacturable structural layout.

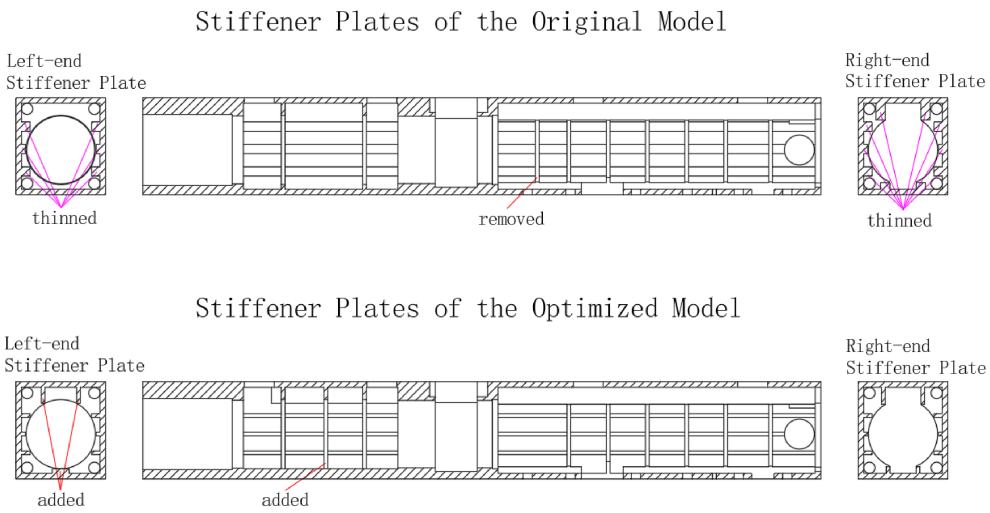


Figure 9. Schematic diagram of ram stiffener reconstruction based on topology optimization results.

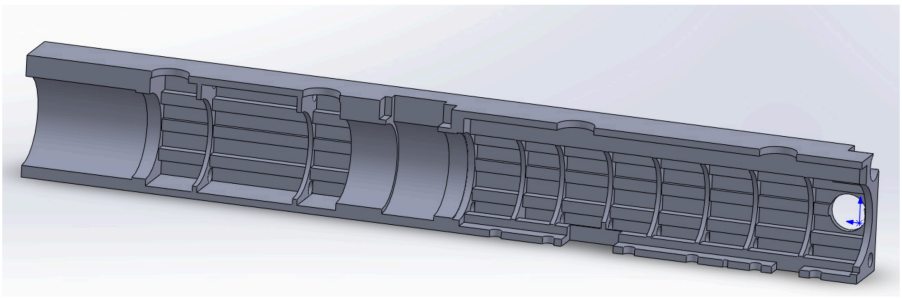


Figure 10. Reconstructed stiffener structure of the ram based on topology optimization results.

To verify the optimization effect, a finite element model of the optimized ram-boring spindle assembly was established while keeping the external dimensions, material properties and assembly relationship unchanged. The reconstructed model was discretized using the same meshing strategy as the original model and contained 806,115 nodes and 422,644 elements. To ensure the comparability of the results before and after optimization, the optimized model adopted the same meshing method, bonded contact relationship at the guideway, fixed constraint at the bottom of the headstock and gravity loading condition as the original model. Only the internal stiffener form, local stiffener number and thickness distribution of the ram were changed. Through this treatment, the influences of material parameters, constraint conditions and loading conditions on the calculation results were excluded, so that the variations in deformation, mass and modal performance before and after optimization mainly resulted from the adjustment of the internal stiffener structure. Static analysis and modal analysis were then carried out for the optimized structure and compared with those of the original structure to verify the effectiveness of topology optimization and engineering reconstruction in reducing ram deflection and improving structural dynamic performance.

4. Performance Verification of the Optimized Structure

4.1. Static Deformation and Displacement Test Verification

To verify the effect of topology optimization and stiffener reconstruction on ram deflection control, static comparative analyses of the original and optimized structures were carried out under the same gravity loading and boundary conditions. The deformation contour of the optimized structure when the ram and boring spindle were both fully extended is shown in Figure 11. Compared with the original structure, the optimized structure exhibited a similar overall deformation distribution. The maximum deformation occurred at the free end of the boring spindle, and the displacement gradually decreased from the boring spindle front end to the headstock support region, showing a typical cantilever bending characteristic. The maximum total deformation decreased from 0.10268 mm in the original structure to 0.097325 mm after optimization, corresponding to a reduction of approximately 5.22%. Meanwhile, the structural mass decreased from 2424 kg to 2363 kg, corresponding to a mass reduction of approximately 2.52%.

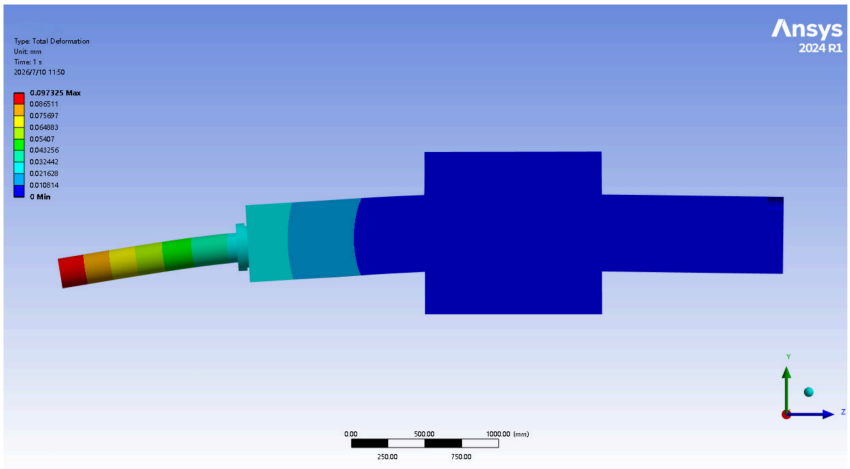


Figure 11. Gravity-induced deformation contour of the optimized structure when the ram and boring spindle are both fully extended.

The simultaneous reductions in structural mass and gravity-induced deformation indicate that the reconstructed stiffener layout provides more effective material distribution and deformation control under large-extension conditions. These improvements can be

attributed to the conversion of the original square stiffener structure into a circular stiffener structure, the addition of longitudinal and circular stiffeners in the front section of the ram, and the appropriate reduction in the thickness of the rear and non-critical stiffeners. After optimization, the newly added longitudinal stiffeners and circular stiffener structure in the front section of the ram jointly improved the sectional support capacity of the overhanging part, allowing the front-end load to be transferred more continuously to the headstock support region. Meanwhile, the reduction in stiffener thickness in the rear and non-critical regions decreased the proportion of inefficient material and concentrated the material distribution in regions that contributed more to bending stiffness. Therefore, the stiffener reconstruction based on topology optimization results can more reasonably allocate the internal material of the ram, improve the structural load transfer path, and enhance the end deformation control capability under large-extension conditions.

The optimized ram was manufactured based on the reconstructed stiffener structure, as shown in Figure 12a. It can be seen that, while the overall external dimensions, mounting interfaces and key mating regions remained unchanged, the internal stiffener form, local stiffener number and thickness distribution of the optimized ram were redesigned, indicating that the engineering reconstruction scheme based on topology optimization results is manufacturable. To verify the end deformation control effect of the optimized structure under the actual assembly condition, a displacement test setup was established on the machine tool, as shown in Figure 12b. During the test, the fixed region of the machine tool was used as the measurement reference, and the displacement measuring device was arranged at the boring spindle front end. The vertical displacement at the boring spindle front end was recorded under different extension conditions. Since the boring spindle front end is close to the tool mounting position, its displacement variation can reflect the end positional deviation of the ram-boring spindle assembly under gravity and further affect the position accuracy of the tool center point. Therefore, it can be used as an important indicator for evaluating the accuracy retention capability of the ram. To ensure the comparability of the test results, the same measuring position, extension conditions and measurement method were adopted for the original and optimized structures. The vertical displacement was measured using a dial indicator with a resolution of 0.001 mm, and the corresponding reading uncertainty was taken as $\pm$0.001 mm.

The simulated and experimental vertical displacements at the boring spindle front end under different extension conditions are listed in Table 1. As shown in Table 1, when the ram was kept at its maximum extension and the boring spindle was gradually extended from 0 mm to 1200 mm, the vertical displacement at the boring spindle front end increased gradually for both the original and optimized structures. For the original structure, the simulated displacement increased from 0.019947 mm to 0.10268 mm, while the experimental displacement increased from 0.021 mm to 0.114 mm. For the optimized structure, the simulated displacement increased from 0.018405 mm to 0.097325 mm, while the experimental displacement increased from 0.019 mm to 0.108 mm. Compared with the original structure, both the simulated and experimental displacements of the optimized structure were reduced under this group of conditions, indicating that the stiffener reconstruction improved the support capability of the ram for the boring spindle front end.

In the second extension mode, where the boring spindle was kept at its maximum extension and the ram was gradually extended, the vertical displacement at the boring spindle front end also increased with increasing ram extension. For the original structure, the simulated displacement increased from 0.038042 mm to 0.10268 mm, while the experimental displacement increased from 0.040 mm to 0.114 mm. For the optimized structure, the simulated displacement increased from 0.037664 mm to 0.097325 mm, while the experimental displacement increased from 0.039 mm to 0.108 mm. Compared with the original

structure, the optimized structure also showed smaller end vertical displacement under this condition, and the reduction became more evident in the large-extension range. When both the ram and boring spindle reached their maximum extensions, the simulated vertical displacement at the boring spindle front end decreased from 0.10268 mm to 0.097325 mm, corresponding to a reduction of approximately 5.22%. The measured displacement decreased from 0.114 mm to 0.108 mm, corresponding to a reduction of approximately 5.26%. The experimental values were slightly higher than the simulated values, mainly because the finite element model involved necessary simplifications, including the omission of non-critical geometric details and the idealization of the guideway support, boundary conditions and assembly relationships. Nevertheless, the simulated and measured results exhibited consistent variation trends, and the calculated and experimentally measured displacement-reduction ratios were close, indicating that the finite element model can reasonably capture the relative change in the structural deformation response and verify the effectiveness of the stiffener reconstruction under large-extension conditions.

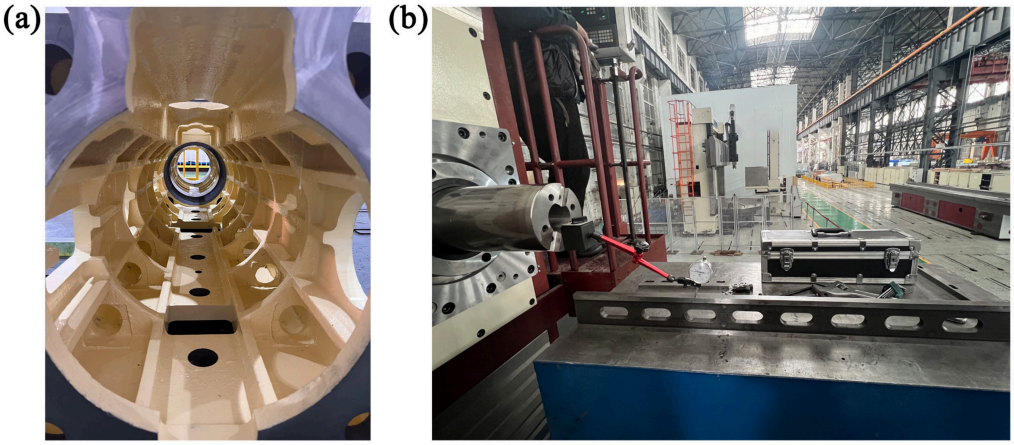


Figure 12. Optimized ram and displacement test setup: (**a**) manufactured optimized ram; (**b**) displacement test setup.

Table 1. Simulated and experimental vertical displacement at the boring spindle front end under different extension conditions before and after optimization (mm).

Mode	Structure	Data	Extension Length of Moving Component (mm)						
			0	200	400	600	800	1000	1200
I	Original	FEM	0.019947	0.024827	0.031026	0.039699	0.052683	0.072434	0.10268
I	Original	Test	0.021	0.027	0.036	0.045	0.056	0.080	0.114
I	Optimized	FEM	0.018405	0.022868	0.028580	0.036685	0.049007	0.067991	0.097325
I	Optimized	Test	0.019	0.024	0.033	0.040	0.052	0.073	0.108
II	Original	FEM	0.038042	0.040037	0.043873	0.051512	0.064822	0.082502	0.10268
II	Original	Test	0.040	0.045	0.050	0.058	0.073	0.091	0.114
II	Optimized	FEM	0.037664	0.039736	0.043662	0.051044	0.063216	0.078634	0.097325
II	Optimized	Test	0.039	0.042	0.049	0.056	0.069	0.085	0.108

Note: Mode I: the ram is kept at its maximum extension, and the boring spindle is gradually extended. Mode II: the boring spindle is kept at its maximum extension, and the ram is gradually extended. FEM represents finite element simulation, and Test represents displacement measurement.

4.2. Modal Performance Verification

Modal analysis was performed on the original and reconstructed structures to evaluate the influence of stiffener reconstruction on the low-order dynamic characteristics of the ram-boring spindle assembly. The first six natural frequencies and mode shape descriptions before and after optimization are listed in Table 2, and the corresponding mode shapes are

shown in Figure 13. As shown in Table 2, the first six natural frequencies of the optimized structure all increased. Specifically, the first natural frequency increased from 177.01 Hz to 184.10 Hz, and the second natural frequency increased from 182.85 Hz to 192.46 Hz, corresponding to increases of approximately 4.01% and 5.26%, respectively.

Table 2. First six natural frequencies and mode-shape descriptions of the original and optimized ram-boring spindle assemblies.

Mode	Original/Hz	Optimized/Hz	Increase/%	Mode Shape Description
1	177.01	184.10	4.01	Boring spindle swings along the X-axis
2	182.85	192.46	5.26	Boring spindle swings along the Z-axis
3	218.99	223.64	2.12	Boring spindle and ram swing together along the X-axis
4	232.90	236.35	1.48	Boring spindle and ram swing together along the Z-axis
5	401.97	420.44	4.60	Slight swing of the boring spindle front end along the X-axis, accompanied by swing of the ram rear end along the X-axis
6	407.41	431.49	5.91	Slight swing of the boring spindle front end along the Z-axis, accompanied by swing of the ram rear end along the Z-axis

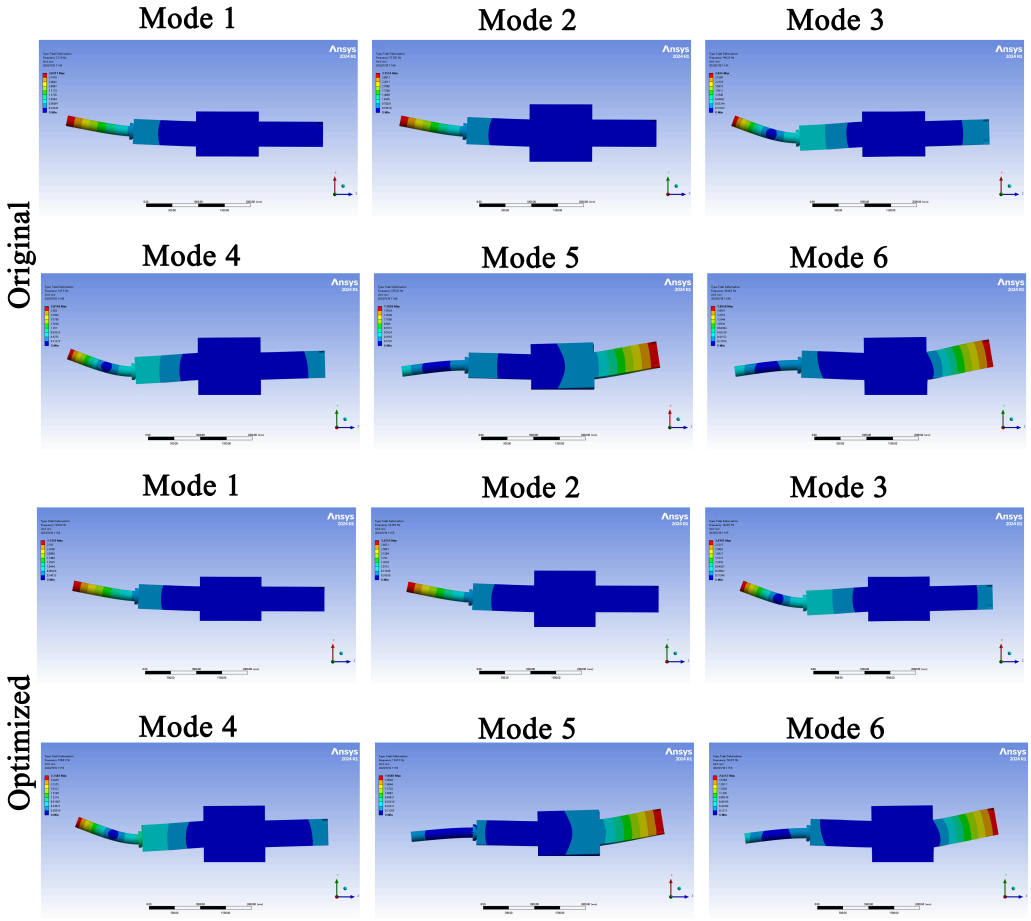


Figure 13. First six mode shapes of the ram-boring spindle assembly before and after optimization.

5. Conclusions

In this study, a ram-boring spindle assembly of a floor-type milling and boring machine was investigated to address the flexural deformation of the ram and the positional deviation at the boring spindle front end under large-extension conditions. A finite element model was established to analyze the gravity-induced deformation and the variation in vertical displacement at the boring spindle front end under different extension conditions. Based on the topology optimization results, the internal stiffener structure of the ram was reconstructed. The main conclusions are as follows:

(1) Under the simultaneous maximum-extension condition, the ram-boring spindle assembly exhibits an obvious cantilever-bending characteristic, and the maximum total deformation occurs at the boring-spindle front end. The vertical displacement at the boring-spindle front end increases with the extension length of either the ram or the boring spindle. When the ram was kept at its maximum extension and the boring spindle was gradually extended, the vertical displacement at the boring spindle front end of the original structure increased from 0.019947 mm to 0.10268 mm. When the boring spindle was kept at its maximum extension and the ram was gradually extended, the vertical displacement increased from 0.038042 mm to 0.10268 mm. These results demonstrate that the front-end deformation is strongly dependent on the extension length, particularly under large-extension conditions.

(2) The deformation characteristics under different extension conditions and the topology–density distribution were jointly used to guide the engineering reconstruction of the internal stiffeners. Relatively high-density regions were observed in the front overhanging section and near the guideway-supported region, whereas relatively low-density regions appeared in part of the rear section. Based on these results, together with casting, assembly, internal space requirements, and engineering experience, three longitudinal stiffeners and one circular stiffener were added in the front section, while selected rear stiffeners were thinned and one circular stiffener was removed. The resulting layout retained the functional interfaces of the original ram and satisfied the requirements of casting and internal assembly.

(3) The static analysis results show that, under the simultaneous maximum extension of the ram and boring spindle, the maximum total deformation decreased from 0.10268 mm to 0.097325 mm after optimization, corresponding to a reduction of approximately 5.22%. The structural mass decreased from 2424 kg to 2363 kg, corresponding to a mass reduction of approximately 2.52%. The displacement test results show that the measured vertical displacement at the boring spindle front end under the maximum extension condition decreased from 0.114 mm to 0.108 mm, corresponding to a reduction of approximately 5.26%. The experimental results are consistent with the finite element results in terms of variation trend and optimization effect, verifying the effectiveness of topology optimization and stiffener reconstruction in reducing end deformation under large-extension conditions.

(4) The modal analysis results show that the first six natural frequencies of the ram-boring spindle assembly all increased after optimization. The first natural frequency increased from 177.01 Hz to 184.10 Hz, and the second natural frequency increased from 182.85 Hz to 192.46 Hz. The improvement range of the first six natural frequencies was 1.48–5.91%. The main mode shape types did not change significantly before and after optimization, indicating that the stiffener reconstruction did not introduce new low-order weak modes while reducing end deformation and structural mass, and improved the low-order dynamic performance of the structure.

Author Contributions: Conceptualization, D.X. and Y.G.; methodology, C.J.; software, R.F.; validation, D.X., and C.J.; formal analysis, R.F.; investigation, Y.G.; resources, D.X.; data curation, R.F.; writing—original draft preparation, R.F.; writing—review and editing, D.X.; visualization, D.X.; supervision, C.J.; project administration, D.X.; funding acquisition, D.X. All authors have read and agreed to the published version of the manuscript.

Funding: This research was funded by Scientific Research Project of Basic Scientific Research Funds in Heilongjiang Provincial Colleges and Universities, grant number 145409317.

Data Availability Statement: The original contributions presented in this study are included in the article. Further inquiries can be directed to the corresponding author.

Conflicts of Interest: Author Chongmin Jiang was employed by the company Genertec Qiqihar No. 2 Machine Tool Co., Ltd. The remaining authors declare that the research was conducted in the absence of any commercial or financial relationships that could be construed as potential conflicts of interest.

References

1. Wu, F.; Wang, S.; Yang, Y.; Wang, Y. Research on deflection compensation of ram of super-heavy-duty CNC floor boring and milling machine. *China Mech. Eng.* **2010**, *21*, 2416–2420. (In Chinese)
2. Wu, F.; Qiao, L.; Xu, Y. Deformation compensation of ram components of super-heavy-duty CNC floor type boring and milling machine. *Chin. J. Aeronaut.* **2012**, *25*, 269–275. [CrossRef]
3. Wu, F.; Zhao, F. A compensation method for deflection of ram with combined pull and push rods. *China Mech. Eng.* **2012**, *23*, 2667–2670, 2684. (In Chinese)
4. Han, Z.; Wang, H.; Shao, Z.; Fu, H.; Jiang, H.; Wang, W. Finite difference method-based calculation of gravity deformation curve for the large-span beam of heavy-duty vertical lathe. *Adv. Mech. Eng.* **2016**, *8*, 1687814016646072. [CrossRef]
5. Zhang, Z.; Jiang, F.; Luo, M.; Wu, B.; Zhang, D.; Tang, K. Geometric error measuring, modeling, and compensation for CNC machine tools: A review. *Chin. J. Aeronaut.* **2024**, *37*, 163–198. [CrossRef]
6. Geng, Z.; Tong, Z.; Jiang, X. Review of geometric error measurement and compensation techniques of ultra-precision machine tools. *Light Adv. Manuf.* **2021**, *2*, 211–227. [CrossRef]
7. Seid Ahmed, Y.; Yu, M.; Chen, F. Advances in computer numerical control geometric error compensation: Integrating AI and on-machine technologies for ultra-precision manufacturing. *Machines* **2025**, *13*, 140. [CrossRef]
8. Bai, Y.; Yuan, Z.; Yan, Y.; Liu, S. Multiobjective optimization for the bed structure of a CNC gantry machine tool based on neural networks and intelligent optimization algorithms. *Sci. Prog.* **2025**, *108*, 00368504251359073. [CrossRef] [PubMed]
9. Lin, S.-Y.; Chang, S.-L. Structure design improvement and stiffness reinforcement of a machine tool through topology optimization based on machining characteristics. *Appl. Sci.* **2024**, *14*, 61.
10. Behera, R.; Chan, T.-C.; Yang, J.-S. Innovative structural optimization and dynamic performance enhancement of high-precision five-axis machine tools. *J. Manuf. Mater. Process.* **2024**, *8*, 181. [CrossRef]
11. Liu, H.; Qiu, Z.; Shi, J.; Sun, J.; Zhang, S. Ground structure method-based stiffener layout topology optimization for horizontal machining center headstock cover plate. *Comput. Struct.* **2025**, *307*, 107633. [CrossRef]
12. Chan, T.-C.; Shao, X.-Y.; Ullah, A.; Farooq, U. Intelligent evolution and enhancing five-axis gantry-type spatial motion structure for Industry 4.0 manufacturing. *Int. J. Adv. Manuf. Technol.* **2024**, *133*, 1965–1990. [CrossRef]
13. Wang, H.; Li, T.; Sun, X.; Mynors, D.; Wu, T. Optimal Design Method for Static Precision of Heavy-Duty Vertical Machining Center Based on Gravity Deformation Error Modelling. *Processes* **2022**, *10*, 1930. [CrossRef]
14. Bilgili, D.; Budak, E.; Altintas, Y. Multibody Dynamic Modeling of Five-Axis Machine Tools with Improved Efficiency. *Mech. Syst. Signal Process.* **2022**, *171*, 108645. [CrossRef]
15. Liu, Y.-P.; Altintas, Y. Predicting the Position-Dependent Dynamics of Machine Tools Using Progressive Network. *Precis. Eng.* **2022**, *73*, 409–422. [CrossRef]
16. Zhuang, Z.-W.; Lu, J.-C.; Liu, D.-S. A Novel Identification Technique of Machine Tool Support Stiffness under the Variance of Structural Weight. *Int. J. Adv. Manuf. Technol.* **2022**, *119*, 247–259. [CrossRef]
17. Jin, B.; Tian, K.; Huang, L. Parametric Reconstruction Method for Topology Optimization Results of Curved Stiffened Structures. *Acta Aeronaut. Astronaut. Sin.* **2024**, *45*, 630586.
18. Busch, P.; Lorenz, M.; Schleicher, P.; Bauernhansl, T. Methodology for Transferring Topology Optimization Results into a Production- and Lightweight-Oriented Differential Design. *Proc. Des. Soc.* **2025**, *5*, 2421–2430. [CrossRef]
19. Guo, Q. Reviews on the Machining and Measurement of Large Components. *Adv. Mech. Eng.* **2023**, *15*, 16878132231191381. [CrossRef]
20. Wang, L.; Han, J.; Tang, Z.; Zhang, Y.; Wang, D.; Li, X. Geometric Accuracy Design of High Performance CNC Machine Tools: Modeling, Analysis, and Optimization. *Chin. J. Mech. Eng.* **2025**, *38*, 87. [CrossRef]
21. Basar, G.; Der, O.; Kahraman, F.; Önder, S. Optimization of hole quality in drilling of direct hot-pressed Al/SiC composites using Taguchi method. *Sci. Rep.* **2026**, *16*, 13591. [CrossRef] [PubMed]
22. Gajević, S.; Miladinović, S.; Güler, O.; Özkaya, S.; Stojanović, B. Optimization of dry sliding wear in hot-pressed Al/B4C metal matrix composites using Taguchi method and ANN. *Materials* **2024**, *17*, 4056. [CrossRef] [PubMed]
23. Slamani, M.; Mayer, R.; Balazinski, M. Concept for the integration of geometric and servo dynamic errors for predicting volumetric errors in five-axis high-speed machine tools: An application on a XYC three-axis motion trajectory using programmed end point constraint measurements. *Int. J. Adv. Manuf. Technol.* **2013**, *65*, 1669–1679. [CrossRef]
24. Slamani, M.; Chatelain, J.-F.; Il, A.; Balazinski, M. Statistical analysis and modeling of temperature distribution during various milling operations of thin-walled aircraft parts. *Phys. A Stat. Mech. Appl.* **2021**, *570*, 125842. [CrossRef]

25. Mechta, A.; Slamani, M.; Zaoui, M.; Mayer, R.; Chatelain, J.-F. Correlation assessment and modeling of intra-axis errors of prismatic axes for CNC machine tools. *Int. J. Adv. Manuf. Technol.* **2022**, *120*, 5093–5115. [CrossRef]
26. Slamani, M.; Mayer, J.R.R.; Balazinski, M.; Carrier, B.; Engin, S. Improvement to high-speed end mill boring accuracy by a simple compensation strategy. *Mach. Sci. Technol.* **2012**, *16*, 1–19. [CrossRef]
27. Slamani, M.; Mayer, J.R.R.; Balazinski, M.; Engin, S. Identification and compensation of dynamic scale mismatches in high-speed end mill boring trajectory on CNC machines. *J. Manuf. Sci. Eng.* **2010**, *132*, 034501. [CrossRef]

Disclaimer/Publisher's Note: The statements, opinions and data contained in all publications are solely those of the individual author(s) and contributor(s) and not of MDPI and/or the editor(s). MDPI and/or the editor(s) disclaim responsibility for any injury to people or property resulting from any ideas, methods, instructions or products referred to in the content.